Journal of Thermal Analysis and Calorimetry, Vol. 92 (2008) 3, 765–769

THERMAL DECOMPOSITION OF AMMONIUM PERCHLORATE ACTIVATED VIA ADDITION OF NiO NANOCRYSTALS

L.-J. Chen, G.-S. Li, P. Qi and L.-P. Li[*]

State Key Lab of Structural Chemistry, Fujian Institute of Research on the Structure of Matter and Graduate School of the Chinese Academy of Sciences, Fuzhou 350002, P.R. China

This work reported on the thermal decomposition of ammonium perchlorate activated by addition of NiO nanocrystals with different surface areas. NiO samples were characterized by X-ray diffraction (XRD), transition electron microscope (TEM), Brunauer–Emmett–Teller (BET) technique, Fourier transform infrared spectroscopy (FTIR), and Raman spectroscopy. With increasing annealing temperature, the surface areas of NiO samples reduced from 108.6 to 0.9 $m^2 g^{-1}$. The catalytic activities of NiO nanocrystals on the thermal decomposition of ammonium perchlorate were investigated by thermogravimetric analysis (TG) coupled with differential thermal analysis (DTA). With addition of NiO nanocrystals, thermal decomposition temperature of AP decreased greatly. Larger surface areas of NiO nanocrystals promoted the thermal decomposition of AP.

Keywords: *ammonium perchlorate, catalysis, NiO nanocrystals, thermal decomposition*

Introduction

Ammonium perchlorate (AP) is one of the main oxidizing agents in composite solid propellants, in which AP plays a significant role in the burning process of the propellant [1]. The burning rate of AP is modified by the addition of small amount of additives [2, 3]. Transition metal oxides including CuO, MgO, Fe_2O_3 [4–6], and their mixtures are most effective and commonly used burn rate additives in practical application of composite solid propellants. These additives can promote the thermal decomposition rate of AP greatly. However, the underlying mechanism of additives on the thermal decomposition of AP is still unclear. Some thought that oxides and AP could easily form the melting eutectics, in which the transition from solid to liquid accelerates the thermal decomposition rate of AP [7]. Others ascribed the catalytic activities of additives to the formation of the intermediate amine compounds [8]. Survase *et al.* proposed an electron based transfer mechanism, in which p-type nanocrystals accept the electrons transferred from perchlorate ions thus enhancing the thermal decomposition of AP [9]. It is also concluded that addition of catalysts can enhance the proton transfer in the thermal decomposition process of AP [10].

Therefore, it is important to systematically study the mechanism of oxide nanoparticle additives on the thermal decomposition of AP. Luo *et al*. thought the average size of CuO has no influence on the thermal decomposition of AP [11]. But recently we found that the larger surface areas of CuO could promote the decomposition rate of AP [12]. The catalytic activity of NiO nanocrystals is better than the bulk [13]. Till now, there is still lack of reports about the impact of average sizes of oxide NiO nanocrystals on the thermal decomposition of AP. Consequently, the investigation of the effect of the surface areas of NiO nanocrystals on the thermal decomposition of AP is necessary to meet the high techniques or defense purposes, since high burning rate composite propellant and operational time for missiles are highly needed in future.

In the present work, we prepared NiO nanocrystals with different surface areas. The lattice vibrational properties and catalytic activities of NiO nanocrystals on the thermal decomposition of AP were investigated. NiO nanocrystals with larger surface areas were found to be more efficient and active on the thermal decomposition of AP.

Experimental

Nickel oxide nanocrystals were prepared through a two-step process. In the first step, $Ni(OH)_2$ was prepared by a chemical precipitation method. Then NiO nanocrystals with different surface areas were obtained by annealing the precipitation at selected temperature for 3 h in air. Details of the samples preparation are reported elsewhere [14].

The structures of the samples were examined by powder X-ray diffraction using Rigaku DMAX2500

* Author for correspondence: lipingli@fjirsm.ac.cn

1388–6150/$20.00
© 2008 Akadémiai Kiadó, Budapest
Akadémiai Kiadó, Budapest, Hungary
Springer, Dordrecht, The Netherlands

X-ray diffractometer with monochromatized CuK_α radiation (λ=0.15418 nm). The average particle size was calculated by the Scherrer formula. The morphologies of the samples were determined using TEM on a JEM-2010 apparatus with an acceleration voltage of 200 kV. The specific surface areas of NiO nanocrystals were determined from the nitrogen absorption data at liquid nitrogen temperature using BET technique on a Micromeritics ASAP 2000 Surface Area and Porosity Analyzer. Infrared spectra of the samples were recorded with Perkin-Elmer IR spectrophotometer using the KBr pellet technique. Raman spectra were recorded using a JY-HR800 spectrometer with a He–Ne laser. The excitation wavelength is 632.8 nm and output powder is 20 mW.

The catalytic activities of NiO nanocrystals in the thermal decomposition of AP (180 μm) were studied using the STA449C thermal analyzer at a heating rate of 20°C min^{-1} in N_2 atmosphere over the range of 30–500°C. TG experiments were performed using open alumina crucible. AP and NiO nanocrystals were mixed at a mass ratio of 98:2 to prepare the target samples for thermal decomposition analyses. A total sample mass of 1.5 mg was used in all runs. The exhausted gases released during the heating process were examined by mass spectroscopy (Jupiter-QMS 403C Aëolos).

Results and discussion

Figure 1 shows the XRD pattern for NiO nanocrystal after annealing at 350°C. All the diffraction peaks matched well with the standard data of NiO (JCPDS No. 47-1049). With increasing annealing temperature, XRD patterns of NiO nanocrystals are similar except for the narrowed peaks [14]. Inset of Fig. 1 shows the TEM image of NiO nanocrystal after annealing at 350°C. It is seen that NiO nanocrystals consisted of spherical particles, nanorods and some irregular shapes.

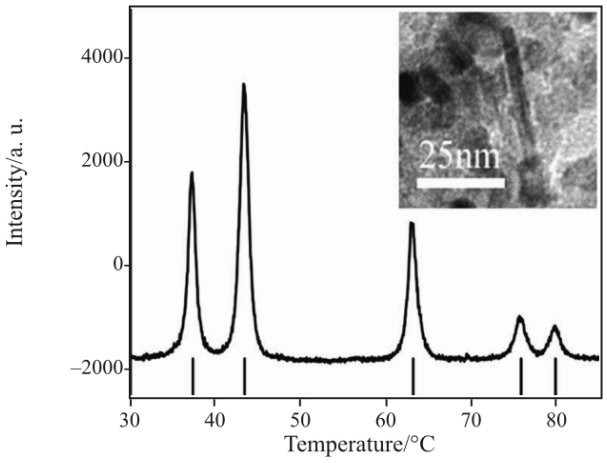

Fig. 1 XRD pattern for NiO nanocrystals after annealing at 350°C. Inset shows the corresponding TEM image. Vertical bars represent the standard diffraction data from JPCDS file for NiO (No. 47-1049)

Since the morphology of NiO was not single uniform morphology, particle sizes calculated from XRD line or TEM are not accurate. In the following, we will address the size effects of NiO nanocrystals using surface areas. The surface areas of NiO nanocrystals were measured by BET technique. NiO nanocrystal after annealing at 350°C has a large surface area of 108.6 m^2 g^{-1}. With increasing the treatment temperatures, surface areas became smaller, e.g., 87.8 m^2 g^{-1} (380°C), 38.1 m^2 g^{-1} (550°C), 26.3 m^2 g^{-1} (600°C), 11.8 m^2 g^{-1} (700°C), 6.8 m^2 g^{-1} (800°C), and 0.9 m^2 g^{-1} (900°C). As for nanostructured materials, the surface area means the ability of adsorption, which has an impact on the catalytic activation of NiO nanocrystals in the thermal decomposition of AP. Generally particle size reduction is followed by structure variation, such as a larger surface to volume ratio and a high concentration of unsaturated bonds on surfaces. Therefore, frequencies of lattice vibration of NiO nanocrystals should vary with particle size.

Lattice vibrations of NiO nanocrystals were studied by IR and Raman spectra. Figure 2 exhibits IR spectra of NiO nanocrystals at different surface areas. An adsorption band at about 435 cm^{-1} was observed for NiO with surface area of 0.9 m^2 g^{-1}, which is assigned to Ni–O stretching vibration mode [15]. With increasing surface area, the Ni–O stretching vibration mode showed a systematic red shift. When the surface area increased to 108.6 m^2 g^{-1}, the Ni-O vibration mode shifted to 407 cm^{-1}. In a previous study, we have shown the particle size dependence of lattice dimension for NiO nanocrystals [14], in which the lattice volume increased when the particle size is smaller than 30 nm (surface

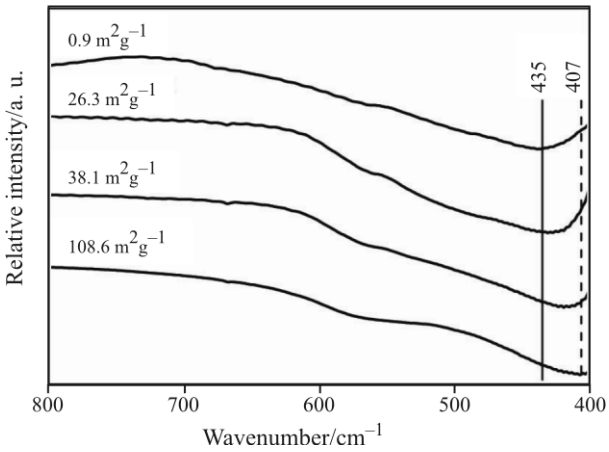

Fig. 2 Infrared spectra of NiO nanocrystals of given surface areas

area 20 $m^2 g^{-1}$). The expansion of lattice volume with increasing surface areas led to the decrease of vibration frequencies of NiO nanocrystals.

Figure 3 shows the Raman spectra of NiO nanocrystals at different surface areas. It can be seen that there are five Raman peaks at 400, 513, 725, 902 and 1093 cm^{-1}, respectively. According to the reference [16], the peaks at 400 and 513 cm^{-1} are assigned to first-order transverse optical (TO) and longitudinal optical (LO) phonon modes of NiO nanocrystals. The peaks at 725 and 1093 cm^{-1} are associated with combination of 2TO and 2LO. The remaining peak at 902 cm^{-1} is assigned to the mixed TO+LO phonon mode. With increasing surface areas, the peaks at 725, 902 and 1093 cm^{-1} disappeared. The main peak at 513 cm^{-1} showed a red shift to 492 cm^{-1} and broadening when the surface area increased to 108.6 $m^2 g^{-1}$. The shift and broadening of LO phonon mode are due to the phonon dispersion that would not be limited to the center of the Brillouin zone with increasing surface area of NiO nanocrystals. Otherwise, the lattice expansion will lead to a red shift of Raman peak [17].

The catalytic activities of NiO nanocrystals were investigated by thermal decomposition of AP. Figure 4 shows the TG curves for pure AP and mixtures of AP and NiO nanocrystals with different surface areas. The decomposition of pure AP is generally centered at temperatures from about 329 to 434°C. Addition of NiO nanocrystals in AP led to a significant reduction of the beginning decomposition and ending decomposition temperature of AP. When adding NiO nanocrystals of surface area of 108.6 $m^2 g^{-1}$, the beginning decomposition temperature reduced to 238.2°C and the ending decomposition temperature reduced to 383°C. This means that the beginning decomposition and ending decomposition temperatures were reduced by 90.8 and 51°C, respectively. When the surface areas of NiO nanocrystal reduced to

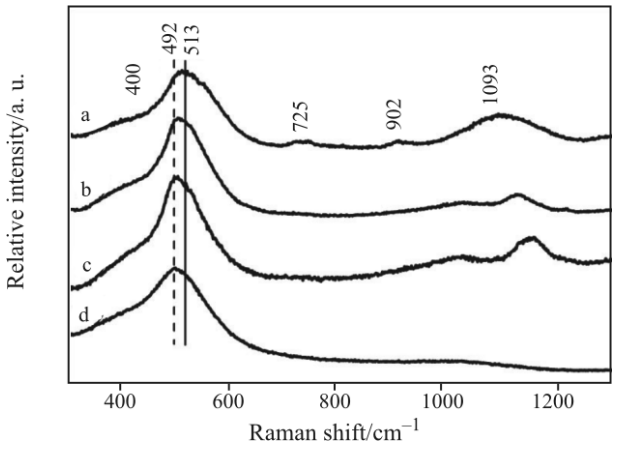

Fig. 3 Raman spectra of NiO nanocrystals of given surface areas; a – 0.9, b – 26.3, c – 38.1 and d – 108.6 $m^2 g^{-1}$

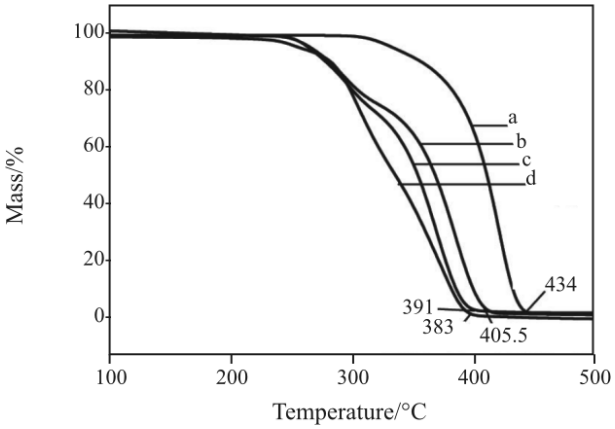

Fig. 4 TG curves for pure AP, mixtures of AP with NiO nanocrystals of different surface areas; a – AP, b – 0.9, c – 6.8 and d – 108.6 $m^2 g^{-1}$

0.9 $m^2 g^{-1}$, the beginning decomposition temperature was decreased by 66°C and the ending decomposition temperature only by 28.5°C.

Figure 5 shows the differential thermal analysis (DTA) curves of pure AP and mixtures of AP with NiO nanopraticles of different surface areas. For pure AP, an endothermic peak was observed at about 250°C, which is assigned to the crystallographic transition of AP from orthorhombic to cubic [18]. With increasing the temperatures, AP underwent two complicated decomposition stages [3], i.e., a low tempera-

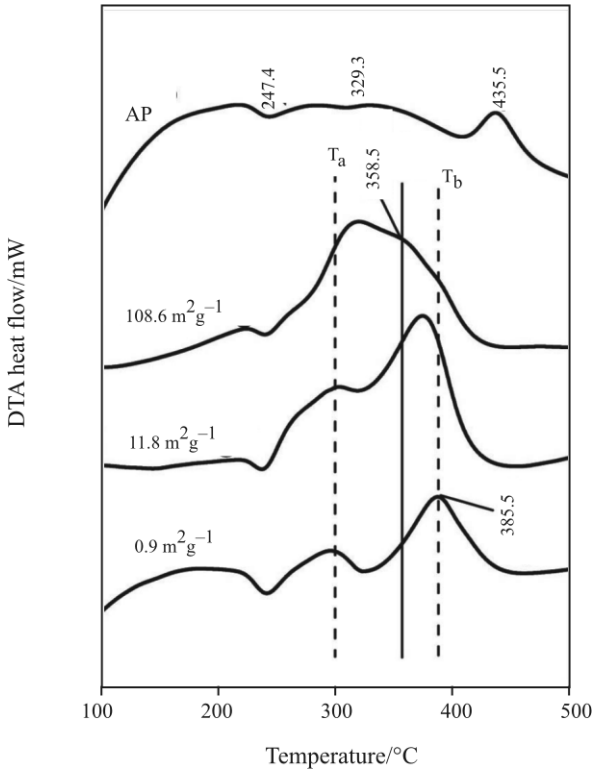

Fig. 5 DTA curves of pure AP and mixtures of AP with NiO nanoparticles of different surface areas

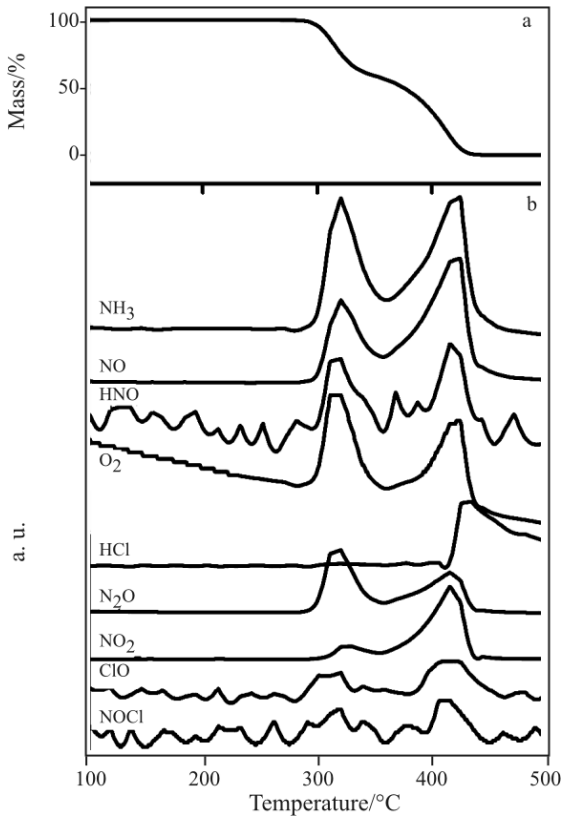

Fig. 6 a – TG curve for pure AP and b – quadrupole mass spectrometry of pure AP

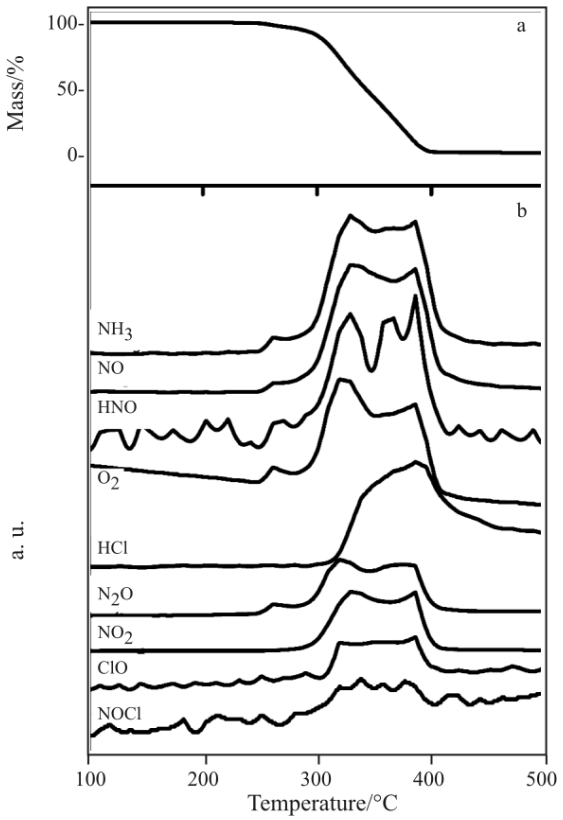

Fig. 7 a – TG curve and b – quadrupole mass spectrometry of mixture of AP with addition of NiO with surface area of 108.6 m^2 g^{-1}

ture stage at 329.3°C and a high temperature stage at 435.5°C, which are followed by two exothermic peaks. These two decomposition stages are consistent with those of 80 μm AP but are apparently different from the single step for 1.1 μm AP [3]. The presence of these NiO nanocrystals slightly lowered the low-temperature decomposition stage of AP (T_a as marked in Fig. 5), while significantly lowered the high-temperature decomposition stage of AP (T_b as shown in Fig. 5). With reducing surface areas from 108.6 to 0.9 m^2 g^{-1}, the high-temperature decomposition peak temperature changed from 358.5 to 385.5°C. The obvious particle size dependence of catalytic activity of NiO nanocrystals in AP decomposition discovered in this work is consistent with our early work [12]. Large surface areas of NiO nanocrystals played a key role in enhancing the catalytic activities in the thermal decomposition of AP.

The catalytic activities of additives on the AP is highly relevant to the thermal decomposition process of AP. Boldyrev [19] proposed that the AP decomposition process is followed by a proton transfer from the cation NH_4^+ to the anion ClO_4^- rather than the electron transfer as reported before, which results in adsorption of ammonia and perchloric acid on the AP surfaces, $NH_4ClO_{4(s)} \rightarrow NH_{3(g)}+HOClO_{3(g)}$ [18, 20]. The key early step is rupture of HO–ClO_3 bond, HO–$ClO_3 \rightarrow$HO+ClO_3. The thermogravimetric analysis (TG) coupled with quadrupole mass spectroscopy (QMS) is an effective method to measure the gases released during the thermal decomposition of AP. Figure 6 shows the TG-QMS of pure AP. The complex thermal decomposition product were NH_3, NO, HNO, O_2, HCl, N_2O, NO_2, ClO and NOCl. Since the thermal decomposition product is highly dependent on the experimental condition, the products can be some different from those reported in reference [18]. HCl is the product of high temperature stage decomposition. Other products exit in both thermal decomposition stages. Figure 7 shows the TG-QMS curves of AP with addition of NiO with surface area of 108.6 m^2 g^{-1}. The products are near the same as those of the pure AP, except that the temperature of high-temperature product lowered.

The TG-QMS data confirmed the formation of ammonium and perchloric acid during the thermal decomposition processes. The high-temperature decomposition stage of AP likely took place at the surfaces of the NiO nanocrystals that involves the adsorption and desorption of ammonium and perchloric acid. Therefore, NiO nanocrystals with a largest surface area of 108.6 m^2 g^{-1} showed the best absorption ability of ammonia and perchloric acid on the surface of AP. While

the low-temperature decomposition stage occurred initially in the pores of nuclei, NiO additives could not easily participate in the proton transfer process. As a result, NiO additives have no apparent impacts on the low temperature decomposition process.

Conclusions

This work explored the thermal decomposition of AP at high temperatures with addition of NiO nanocrystals. NiO nanoparticles with different surface areas were achieved by annealing the $Ni(OH)_2$ at different temperature. With increasing surface areas, both IR spectra and LO Raman peak showed red shift, which is associated with the lattice expansion. NiO nanocrystals promoted AP decomposition, in which the catalytic activities were found to be a function of surface area. The high-temperature decomposition peak temperature in the presence of NiO nanoparticles changed from 358.5 to 385.5°C with surface areas of NiO reduced from 108.6 to 0.9 $m^2 g^{-1}$.

Acknowledgments

This work was financially supported by NSFC under the contract (No. 20773132, 20771101), National Basic Research Program of China (973 program, No. 2007CB613306), Science and Technology Program from Fujian Province (No. 2005L2005 and 2006HJ0178), Directional program (KJCX2-YW-M05) and a grant from Hundreds Youth Talents Program of CAS (Li GS).

References

1 L. Bereczki, K. Marthi, P. Huszthy and G. Pokol, J. Therm. Anal. Cal., 78 (2004) 449.
2 Y. L. Su, S. F. Li and D. H. Ding, J. Therm. Anal. Cal., 86 (2006) 497.
3 J. Zhi, W. Tian-Fang, L. Shu-Fen, Z. Feng-Qi, L. Zi-Ru, Y. Cui-Mei, L. Yang, L. Shang-Wen and Z. Gang-Zhui, J. Therm. Anal. Cal., 85 (2006) 315.
4 N. B. Singh and A. K. Ojha, Thermochim. Acta, 390 (2002) 67.
5 G. R. Duan, X. J. Yang, J. Chen, G. H. Huang, L. Lu and X. Wang, Power Technol., 172 (2007) 27.
6 P. R. Patil, V. N. Krishnamurthy and S. S. Joshi, Prop. Explos. Pyrotech., 31 (2006) 442.
7 F. Solymosi and L. Révész, Nature, 192 (1961) 64.
8 K. C. Patil, V. R. Verneker and S. R. Jain, Combust. Flame, 27 (1976) 295.
9 D. V. Survase, M. Gupta and S. N. Asthana, Prog. Crystal Growth Charact., 45 (2002) 161.
10 R. J. Acheson and P. W. M. Jacobs, J. Phys. Chem., 74 (1970) 281.
11 Y. X. Luo, L. D. Lu, X. H. Liu, X. J. Yang and X. Wang, Chin. J. Inorg. Chem., 18 (2002) 1211.
12 L. J. Chen, G. S. Li and L. P. Li, J. Therm. Anal. Cal., 91 (2008) 581.
13 Y. P. Wang, J. W. Zhu, X. J. Yang, L. Lu and X. Wang, Thermochim. Acta, 437 (2005) 106.
14 L. P. Li, L. J. Chen, R. M. Qihe and G. S. Li, Appl. Phys. Lett., 89 (2006) 134102.
15 L. L. Wu, Y. S. Wu, H. Y. Wei, Y. C. Shi and C. X. Hu, Mater. Lett., 58 (2004) 2700.
16 R. E. Dietz, G. I. Parisot and A. E. Meixner, Phys. Rev. B., 4 (1971) 2302.
17 R. P. Wang, G. W. Zhou, Y. L. Liu, S. H. Pan, H. Z. Zhang, D. P. Yu and Z. Zhang, Phys. Rev. B., 61 (2000) 16827.
18 M. Rajić and M. Sućeska, J. Therm. Anal. Cal., 63 (2001) 375.
19 V. V. Boldyrev, Thermochim. Acta, 443 (2006) 1.
20 P. Politzer and P. Lane, J. Mol. Struct. (Theochem), 454 (1998) 229.

Received: August 6, 2007
Accepted: November 27, 2007

DOI: 10.1007/s10973-007-8678-3